Modeling and Dynamic Analysis of a 9 MW DFIG-Based Grid-Connected Wind Energy Conversion System

Godwin Osariemen Igbinosa, Nosagieagbon Owomano Imarhiagbe*, Urhomweonsa Ohihole Eribo, Gbenga Walter Bolarinwa, Aluko Olawale, and Yusuf Maaji

Department of Electrical, Electronic and Telecommunication Engineering, Bells University of Technology, Ota, Nigeria.
*Corresponding Author Email: noimarhiagbe@bellsuniversity.edu.ng

Direct Research Journal of Engineering and Information Technology

Vol. 14(1), Pp. 58-72, March 2026,

Research Article
ISSN: 2354-4155
https://journals.directresearchpublisher.org/index.php/drjeit; https://www.ajol.info/index.php/drjeit

Received 5 November 2025, Accepted 25 February 2026, Published 6 March 2026

ABSTRACT

The global shift toward low-carbon energy sources has elevated the role of wind power in sustainable electricity generation. This study presents the design and MATLAB/Simulink-based simulation of a 9 MW grid-connected doubly fed induction generator (DFIG) wind energy conversion system. The system comprises a horizontal-axis wind turbine, back-to-back converters, and a DC-link, with decoupled vector control used to regulate active and reactive power. The wind farm is connected to a 120 kV point of common coupling and interfaced with a 575 kV transmission network through step-up transformer stages. System performance is evaluated under normal operating conditions and symmetrical grid faults, with emphasis on transient and steady-state response as well as fault ride-through capability. Sensitivity and correlation analyses identify grid frequency and converter switching frequency as the most influential parameters affecting system performance. The results demonstrate stable operation, effective power quality control, and satisfactory dynamic response, confirming the suitability of DFIG-based wind energy systems for large-scale grid integration. The findings provide practical guidance for optimizing wind power systems and support the deployment of reliable and resilient renewable energy infrastructure in developing regions.

Keywords: *Wind Energy Conversion System (WECS), Doubly Fed Induction Generator, Grid Integration, Vector Control, Field-Oriented Control (FOC), Renewable Energy*

Citation: Igbinosa,G. O., Imarhiagbe, N. O., Eribo, U. O., Bolarinwa, G.W., Olawale, A., & Maaji, Y. (2026). Modeling and Dynamic Analysis of a 9 MW DFIG-Based Grid-Connected Wind Energy Conversion System. *Direct Research Journal of Engineering and Information Technology*, 14(1), Pp. 58-72. https://doi.org/10.26765/DRJEIT18888181

INTRODUCTION

The global transition toward low-carbon power systems has deepened over the past four decades, reflecting an evolution from early concerns over fuel security to clear evidence of climate-related impacts that now drive large-scale renewable deployment. Wind energy has become one of the leading contributors to this transition because of its resource abundance and declining levelized cost of electricity (Wagner, 2018; Yaramasu et al., 2017). As turbine ratings have progressed from early kilowatt-scale units to today's multi-megawatt machines, wind power has shifted from a supplementary source to a critical component of national generation portfolios, creating new technical and operational demands (Desalegn et al., 2022). This evolution shapes both the design priorities and stability requirements of grid-connected Wind Energy Conversion Systems (WECS).

A Grid-Connected WECS (GC-WECS) enables real-time delivery of wind energy to the utility network, supporting voltage and frequency regulation while improving renewable energy utilization (Alhato and Bouallègue, 2021; Hackl et al., 2018). Energy conversion depends on aerodynamic, mechanical, electrical, and converter interactions, with generator choice playing a central role. Among available technologies, the Doubly-Fed Induction Generator (DFIG) has become widely used in multi-MW turbines because of its variable-speed operation, reduced converter ratings, and flexible reactive power control (Yan et al., 2020; Nadour et al., 2017).

As wind farms expand, grid integration challenges become more significant. Large turbines can introduce voltage instability, frequency deviation, harmonic distortion, and vulnerability under disturbed grid conditions. These challenges are amplified in regions with aging or poorly reinforced infrastructure, a pattern documented in empirical studies examining developing-country networks and their asset deterioration trends (Eberhard et al., 2011; Karekezi and Kimani, 2002). This context creates a clear need for advanced control strategies and system-level analyses capable of handling the demands of large-scale DFIG-based WECS.

Modern DFIG systems rely on coordinated control strategies, including MPPT and vector control rather than repeated or separate mentions of similar methods, to regulate power flow and maintain stability (Tiwari and Babu, 2016; Moussa et al., 2019). Back-to-back PWM converters enable decoupled rotor and grid control and support low-voltage ride-through (LVRT) compliance (Elbeji et al., 2014). However, much of the available literature focuses on 1.5–5 MW turbines, leaving a limited body of validated work addressing the behavior, control stress, and grid-interaction characteristics of 8–10 MW DFIG machines. These larger systems exhibit distinct dynamic behaviors due to increased inertia, higher converter ratings, and more complex fault interactions.

As turbine ratings increase, they also require more advanced monitoring and diagnostic capabilities. SCADA-based and intelligent fault-detection systems have therefore become essential for ensuring reliability at these scales (Reddy et al., 2018; Chong et al., 2021). Simulation environments such as MATLAB/Simulink allow detailed modeling of aerodynamics, generator behavior, converters, and grid interfaces (Rajesh et al., 2022; Das and Akella, 2018). Despite rapid global deployment of large turbines, the limited availability of validated studies on 9 MW DFIG configurations represents a clear research gap. This rating is particularly important because it sits at a threshold where converter stress, LVRT behavior, harmonic susceptibility, and mechanical inertia diverge from smaller machines. Many emerging grids are beginning to adopt wind plants at this scale, making performance evaluation both timely and necessary. This study addresses this gap by developing and analyzing a 9 MW grid-connected DFIG-based WECS using MATLAB/Simulink, focusing on its behavior under varying wind conditions and grid disturbances, and on identifying system-level operational limits.

The objectives of the study are:

a. To develop a complete MATLAB/Simulink model of a 9 MW DFIG-based WECS, incorporating turbine aerodynamics, generator dynamics, power electronics, and grid interfacing.
b. To evaluate the system's dynamic response to varying wind conditions and grid disturbances, with attention to power quality, active/reactive power control, and overall stability.
c. To assess the effectiveness of MPPT and vector control strategies in improving conversion efficiency and stable power delivery.
d. To conduct a sensitivity analysis identifying how key mechanical, electrical, and control parameters influence performance.
e. To identify operational limitations—such as LVRT behavior, slip-ring constraints, EMI susceptibility, and harmonic vulnerability and discuss their implications for practical deployment.

The research is guided by the following questions:

i. How does a 9 MW DFIG-WECS perform under varying wind and grid-disturbance conditions?
ii. How effective are MPPT and vector control strategies in improving energy extraction and stability?
iii. Which mechanical, electrical, and control parameters most strongly influence system efficiency and dynamic behavior?
iv. What operational limitations constrain the deployment of large-capacity DFIG systems in real grid environments?

By addressing these issues, the study provides evidence-based insight into the behavior and deployment

requirements of large-capacity DFIG turbines in both developed and emerging power systems.

LITERATURE REVIEW

Evolution of Wind Energy Conversion Systems

Wind Energy Conversion Systems (WECS) have evolved considerably due to advances in turbine aerodynamics, power electronic interfaces, and intelligent control strategies. Modern WECS are designed to achieve high energy conversion efficiency, comply with increasingly stringent grid codes, and maintain stability during grid disturbances (Wagner, 2018; Alhato & Bouallègue, 2019; Desalegn et al., 2022). These developments have enabled improved fault ride-through capability and enhanced control of active and reactive power under variable operating conditions.

Comparative investigations of generator technologies indicate that doubly fed induction generators (DFIGs) and permanent magnet synchronous generators (PMSGs) outperform squirrel cage induction generators (SCIGs) in terms of dynamic response and energy capture, particularly under low and fluctuating wind speeds (Chong et al., 2021; Rajesh et al., 2022). As a result, SCIG-based systems have seen reduced adoption in modern grid-connected applications.

DFIG- and PMSG-Based Wind Energy Systems

DFIG-based WECS remain dominant in onshore installations due to their partial-scale converter architecture, which reduces converter rating and capital cost while enabling independent control of active and reactive power (Das & Akella, 2018). However, the direct stator-to-grid connection inherent in DFIGs increases their sensitivity to grid disturbances. PMSG-based WECS, in contrast, employ full-scale converters that electrically decouple the generator from the grid. This configuration offers superior controllability, improved fault isolation, and reduced mechanical stress, making PMSGs particularly attractive for offshore applications where maintenance access is limited (Morgan et al., 2022). These advantages are offset by higher converter losses and increased upfront cost, highlighting a fundamental trade-off between economic efficiency and fault robustness.

Grid Fault and Fault Ride-Through Studies

Grid-tied WECS commonly utilize back-to-back voltage source converters with vector control strategies to ensure stable operation during grid disturbances. Studies have shown that field-oriented control (FOC) enables accurate torque and reactive power regulation during transient events, supporting grid voltage recovery during faults (Linus & Damodharan, 2015; Peng et al., 2021). Simulation-based platforms such as MATLAB/Simulink are widely adopted to evaluate these control schemes under diverse operating scenarios. In recent years, there has been intensified focus on LVRT and FRT compliance for grid-connected DFIG machines, driven by stringent grid codes that require wind turbines to remain connected during voltage sags and to support system recovery by injecting active and reactive currents. A comprehensive review of LVRT capabilities in WECS highlights not only the challenges posed by voltage dips but also the role of advanced control strategies and fault-ride-through techniques in meeting evolving grid standards. For example, systematic analysis of LVRT techniques for grid-connected DFIG wind turbines classifies approaches based on their effectiveness in different fault scenarios and their alignment with grid code requirements (Kasem et al., 2023).

Specific strategies for enhancing LVRT performance include hardware augmentation and control innovations. An optimal control strategy for low voltage ride-through in doubly-fed wind farms during asymmetrical faults demonstrates that enhanced control schemes can significantly improve LVRT performance and grid support during fault events (Botong et al., 2024). Similarly, recent simulation studies have evaluated the voltage and current dynamics of DFIG systems under symmetrical faults, revealing the transient behavior of stator and rotor currents and the effectiveness of fault-ride-through strategies in maintaining grid connection and mitigating hardware stress (Okeke et al., 2024). Other work explores practical LVRT enhancements, such as the use of series resistors or coordinated reactive power support schemes, to bolster the ride-through performance of grid-connected DFIG models under both symmetrical and asymmetrical fault conditions (Lu et al., 2024). These studies collectively illustrate that while traditional vector control schemes have laid the groundwork, contemporary research emphasizes adaptive and auxiliary techniques to fulfill modern LVRT/FRT requirements.

Taken together, these recent contributions enrich the understanding of LVRT/FRT behavior in DFIG-based systems and underscore the need for fault-aware control design, which remains an active area of research in the WECS community.

Comparative Performance of DFIG and PMSG under Symmetrical Faults

Under symmetrical grid faults, DFIG-based systems exhibit heightened vulnerability due to their partial-scale converters and direct stator-grid coupling, which exposes the rotor circuit to large transient currents (Mosayyebi et al., 2022). Protection mechanisms such as crowbar circuits are typically employed to safeguard the rotor-side converter; however, their activation temporarily disables reactive power control, thereby limiting grid support during critical fault periods.

To protect the rotor-side converter, auxiliary protection schemes such as crowbar circuits and dynamic voltage

support strategies are commonly employed. While effective in limiting rotor currents, crowbar activation forces the DFIG to operate temporarily as a squirrel-cage induction generator, resulting in the loss of reactive power controllability at a time when grid support is most critical. Recent studies show that although advanced control schemes and coordinated protection strategies have improved LVRT compliance, the inherent structural vulnerability of DFIGs under symmetrical faults remains a limiting factor, particularly in weak grids and high-fault-severity scenarios ((Kasem et al., 2023; Botong et al., 2024).

In contrast, PMSG-based WECS benefit from full-scale converter interfaces that electrically decouple the generator from the grid. This explains their superior fault ride-through capability and stable current control during deep voltage sags. Recent comparative studies demonstrate that PMSG systems can maintain controlled active and reactive current injection throughout symmetrical fault events, facilitating faster voltage recovery and reduced electromagnetic stress on the generator (Morgan et al., 2022). However, this improved fault performance is achieved at the expense of higher converter ratings, increased switching losses, and stricter thermal and harmonic constraints, particularly during prolonged fault conditions.

Comparative analyses conducted in recent literature indicate that while both DFIG and PMSG systems can be engineered to satisfy modern LVRT and FRT grid code requirements, they do so through fundamentally different mechanisms. DFIG-based systems rely heavily on coordinated protection and control augmentation to survive symmetrical faults, whereas PMSG-based systems leverage full converter decoupling to inherently withstand grid disturbances. This distinction highlights a critical trade-off between converter complexity, cost, and fault resilience, which remains central to generator selection and control design in modern WECS.

Sensitivity and Correlation Studies in WECS

Beyond fault ride-through capability, recent studies emphasize the importance of sensitivity and correlation analyses in understanding how system parameters influence WECS performance metrics such as voltage stability, rotor speed dynamics, and power flow (Moussa et al., 2019; Reddy et al., 2018). Despite this progress, most existing studies focus on steady-state or limited transient conditions and do not explicitly examine the influence of grid frequency deviations or converter switching frequency.

More recent investigations have extended sensitivity analysis frameworks to grid-connected WECS operating under disturbed conditions. These studies demonstrate that controller gains, phase-locked loop dynamics, and converter-related parameters can significantly affect transient response and fault recovery characteristics, particularly in weak grid environments (Bhowon et al., 2022). Correlation-based approaches have also been employed to identify dominant parameter interactions and reduce model complexity by isolating parameters with negligible impact on system dynamics. Despite these advances, most existing sensitivity studies focus on wind speed variation, mechanical inertia, or controller tuning under nominal grid conditions. The explicit influence of grid frequency deviations on converter control dynamics, as well as the role of converter switching frequency in shaping LCL filter resonance and harmonic distortion during fault events, remains insufficiently explored. This limitation is especially evident in comparative studies involving DFIG- and PMSG-based systems, where switching frequency and frequency-dependent control behavior are often treated as fixed design choices rather than uncertainty-sensitive parameters.

Accordingly, there remains a clear gap in the literature for systematic sensitivity and correlation analyses that explicitly quantify the impact of grid frequency variation and converter switching frequency on fault ride-through performance and power quality. Addressing this gap is critical for developing fault-resilient WECS designs that remain robust under both grid disturbances and parameter uncertainty, which directly motivates the analytical framework adopted in the present study.

METHODOLOGY

The system under study is a grid-connected Wind Energy Conversion System (WECS) comprising a 9 MW horizontal-axis wind turbine, a Doubly-Fed Induction Generator (DFIG), and a back-to-back PWM converter. The system connects to a 575 kV grid and incorporates vector control for active/reactive power regulation. MATLAB/Simulink is used as the simulation environment. A three-phase symmetrical fault is applied at the 120 kV point of common coupling to assess the fault ride-through capability of the DFIG-based wind farm.

System Modelling

The dynamic behavior of the wind energy conversion system is modeled by integrating the aerodynamic characteristics of the wind turbine with the electrical and control dynamics of the doubly fed induction generator (DFIG). The aerodynamic power extracted from the wind is governed by the wind speed, air density, turbine swept area, and power coefficient, as expressed in Equation 1. The operating condition of the turbine is characterized by the tip-speed ratio, defined in Equation 2, which directly links rotor speed to wind velocity. The mechanical torque applied to the generator shaft is subsequently obtained from the extracted power, as given in Equation 3. These equations form the basis for evaluating energy capture and for implementing maximum power point tracking within the simulation model. The generator and converter ratings were constrained to a nominal turbine capacity of 9 MW, and steady-state outputs were verified to remain within

rated limits.

$$P_m = ½\, C_P\, (\lambda, \beta) \rho A V^3 \quad (1)$$

$$\lambda = \frac{\omega R}{V} \quad (2)$$

$$T_m = \frac{P_m}{\omega_r} \quad (3)$$

DFIG Electrical Model

The electrical dynamics of the doubly fed induction generator are modeled using a synchronously rotating d–q reference frame. This representation enables decoupled analysis of active and reactive power and is well suited for vector control implementation. The stator and rotor voltage relationships in the d–q frame are defined by Equations 4 – 7, where resistive drops, flux derivatives, and speed-dependent coupling terms are explicitly accounted for. This formulation allows accurate representation of transient and steady-state behavior under normal and disturbed grid conditions.

$$V_{ds} = R_s I_{ds} + \frac{d\varphi_{ds}}{dt} - \omega_s \varphi_{qs} \quad (4)$$

$$V_{qs} = R_s I_{qs} + \frac{d\varphi_{qs}}{dt} + \omega_s \varphi_{ds} \quad (5)$$

$$V_{dr} = R_r I_{dr} + \frac{d\varphi_{dr}}{dt} - \omega_r \varphi_{qr} \quad (6)$$

$$V_{qr} = R_r I_{qr} + \frac{d\varphi_{qr}}{dt} + \omega_r \varphi_{dr} \quad (7)$$

Flux Linkage Equations

The voltage equations of the DFIG are coupled through the stator and rotor flux linkages, which depend on the self and mutual inductances of the machine. These relationships are expressed in (8)–(11), linking stator and rotor currents to their respective flux components. The inclusion of mutual inductance terms captures the electromagnetic coupling between stator and rotor circuits, which is essential for accurately modeling torque production and power exchange with the grid.

$$\varphi_{ds} = L_S I_{ds} + L_m I_{dr} \quad (1)$$

$$\varphi_{qs} = L_S I_{qs} + L_m I_{qr} \quad (2)$$

$$\varphi_{dr} = L_r I_{dr} + L_m I_{ds} \quad (3)$$

$$\varphi_{dr} = L_r I_{qr} + L_m I_{qs} \quad (4)$$

Power and Torque Equations

The electromagnetic torque developed by the DFIG is derived from the interaction between stator flux and current components in the rotating reference frame. This relationship is defined by Equation 12, where the number of pole pairs determines the torque scaling. The torque equation provides the mechanical–electrical interface required to couple the generator model with the turbine drive-train dynamics and to analyze speed variations during grid disturbances.

$$T_e = \frac{3}{2_p L_m} \left(I_{qs} I_{dr} - I_{ds} I_{qr} \right) \quad (5)$$

where p is the number of pole pairs. The grid's injected active and reactive power is shown in Equations 12 and 13 respectively:

$$P_s = V_{ds} I_{ds} + V_{qs} I_s \quad (6)$$

$$Q_s = V_{qs} I_{ds} - V_{ds} I_{qs} \quad (7)$$

All symbols and parameters used in the wind turbine, generator, and converter models are defined in (Table 1).

Table 1: Definition of Symbols Used in the WECS and DFIG Model.

Symbol	Description	Unit
P_m	Mechanical power extracted from wind	W
ρ	Air density	kg/m³
A	Turbine swept area	m²
C_m	Power coefficient	–
v_w	Wind speed	m/s
λ	Tip-speed ratio	–
ω_r	Rotor angular speed	rad/s
R	Turbine blade radius	m
T_m	Mechanical torque	N·m
v_{ds}, v_{qs}	Stator voltages (d–q axes)	V
v_{dr}, v_{qr}	Rotor voltages (d–q axes)	V
i_{ds}, i_{qs}	Stator currents (d–q axes)	A
i_{dr}, i_{qr}	Rotor currents (d–q axes)	A
ψ_{ds}, ψ_{qs}	Stator flux linkages	Wb
ψ_{dr}, ψ_{qr}	Rotor flux linkages	Wb
R_s, R_r	Stator and rotor resistances	Ω
L_s, L_r	Stator and rotor inductances	H
L_m	Mutual inductance	H
ω_s	Synchronous angular speed	rad/s
p	Number of pole pairs	–
T_e	Electromagnetic torque	N·m
V_{dc}	DC-link voltage	V
C	DC-link capacitance	F
f_g	Grid frequency	Hz
f_{sw}	Converter switching frequency	Hz

Maximum Power Point Tracking Strategy

To ensure maximum energy extraction from the available wind resource, a speed-based maximum power point tracking (MPPT) strategy is employed in this study. The adopted approach is based on maintaining the turbine operation at its optimal tip-speed ratio, which corresponds to the maximum power coefficient of the wind turbine. Under variable wind conditions, the reference generator speed is adjusted according to the wind speed such that the turbine operates along the optimal power–speed

characteristic. This control principle allows the aerodynamic efficiency of the turbine to be maximized without the need for direct power optimization algorithms or real-time estimation of the power coefficient. As a result, the MPPT strategy remains computationally efficient and well suited for dynamic simulation studies. The generator speed serves as the primary controlled variable in the MPPT implementation. By regulating the electromagnetic torque through the rotor-side converter, the generator speed is driven to track its optimal reference value derived from the turbine power–speed relationship. This torque speed coordination ensures that the mechanical power extracted from the wind is maximized prior to grid interaction. The MPPT strategy is directly linked to the aerodynamic turbine model described in Section 3.1, where the power coefficient is defined as a function of the tip-speed ratio and blade pitch angle. During normal operation, the pitch angle is held constant to enable maximum power extraction, while the MPPT controller regulates generator speed to maintain optimal turbine operation. At higher wind speeds or during grid disturbances, turbine operation is governed by converter and protection constraints, and MPPT action is temporarily overridden to preserve system stability.

During grid disturbance conditions such as symmetrical voltage dips, the MPPT loop is temporarily deactivated to prevent instability caused by rapid torque demand under reduced stator voltage. In such events, the rotor-side converter transitions from speed-tracking mode to current-limiting vector control mode in order to maintain converter ratings and support reactive power injection for voltage recovery. Once grid voltage is restored to its nominal range, MPPT operation is automatically resumed and generator speed is driven back to the optimal reference. This coordinated switching between MPPT-based speed control and fault-ride-through current control ensures that aerodynamic efficiency is maximized during normal operation while electrical stability is preserved during fault transients.

Rotor-Side Converter (RSC) Control

The rotor-side converter is responsible for controlling the generator electromagnetic torque and reactive power by regulating the rotor current components. The control objectives for active and reactive power are implemented through current reference generation and tracking, as represented by the control expressions in Equations 14 and 15. This strategy enables independent control of stator active and reactive power while supporting grid code requirements during normal operation and fault conditions.

$$P_s = \frac{3}{2(V_{ds}I_{ds} + V_{qs}I_{qs})} \quad (8)$$

$$Q_s = \frac{3}{2(V_{qs}I_{ds} - V_{ds}V_{qs})} \quad (9)$$

Grid-Side Converter (GSC) Control

The grid-side converter maintains the DC-link voltage at a constant reference value to ensure stable power exchange between the rotor circuit and the grid. The dynamic behavior of the DC-link capacitor is described by (17), which relates the capacitor voltage to the power imbalance between the rotor-side and grid-side converters. Proper regulation of the DC-link voltage is critical for preventing overvoltage during grid disturbances and ensuring converter stability.

$$\frac{C_d V_{dc}}{d_t} = P_g - \frac{P_{load}}{V_{dc}} \quad (10)$$

Detailed model for Doubly Fed Induction Generator

As shown in (Figure 1), the wind farm consists of six 1.5 MW wind turbines equipped with doubly fed induction generators and connected to a 25 kV collection network. The generated power is transmitted over a 25 kV feeder and stepped up to a 120 kV point of common coupling, from which it is interfaced with the 575 kV transmission system through step-up transformer stages. Figure 1 presents a schematic representation of the overall system configuration. A three-phase symmetrical fault is applied at the 120 kV point of common coupling to assess the fault ride-through capability of the DFIG-based wind farm.

Simulation Parameters and Operating Conditions

The modeling methodology consists of the incorporation of certain Simulink blocks of Simscape Electrical library, whose parameters have been set based on conventional electrical engineering techniques, as well as attachment components, as illustrated in (Table 2). The wind farm consists of six identical 1.5 MW turbines, resulting in a total installed capacity of 9 MW.

Simulations were performed in MATLAB/Simulink using a detailed time-domain model of the grid-connected wind energy conversion system, incorporating the aerodynamic turbine model, generator–converter dynamics, control loops, and grid interface. A nominal wind speed of 15 m/s was used as the base operating point, with controlled variations introduced in line with the sensitivity analysis ranges. The grid was modeled as a balanced three-phase system operating at 50 Hz, with symmetrical voltage faults applied to assess fault ride-through behavior. Grid frequency deviations were also introduced to evaluate their impact on converter control and power recovery. The back-to-back voltage source converter was implemented using PWM, with switching frequency treated as a variable parameter to examine its influence on harmonic behavior and dynamic response. All simulations employed a fixed-step discrete solver with a sampling time selected to accurately capture switching and control dynamics. Each case was initialized under steady-state conditions, and

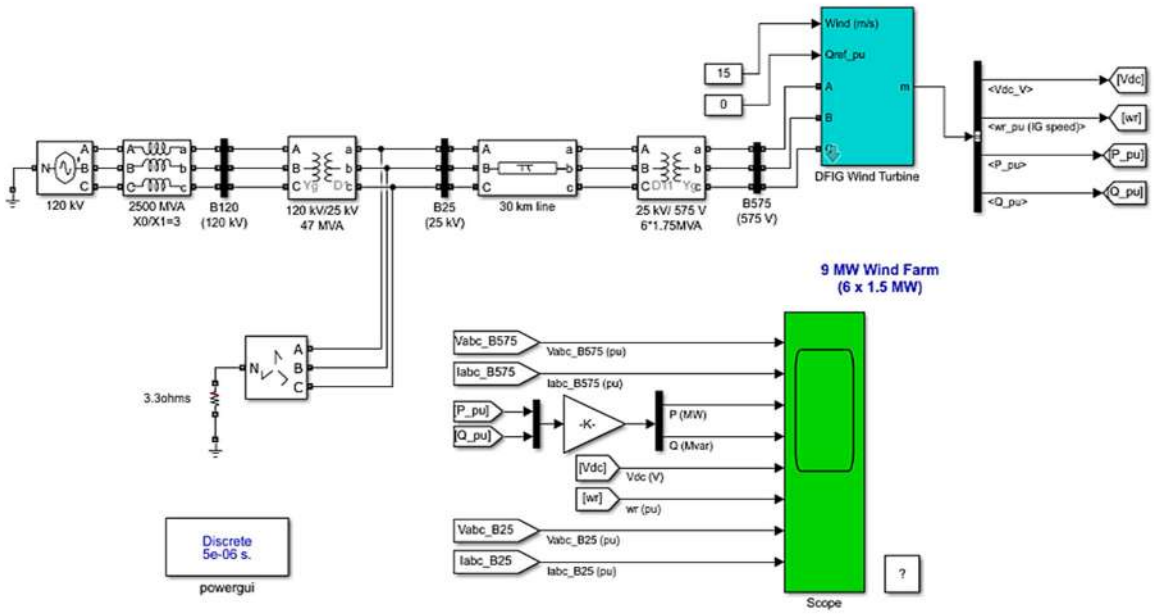

Figure 1: System Model of Wind Energy Conversion System.

Table 2: Component parameter.

Component	Parameter	Value
Grid Source	PCC voltage level / Transmission grid voltage	120 kV / 575 kV
	Frequency	50Hz
	Short-circuit level	2500MVA
	Positive-sequence reactance	5.76 ohms
	Zero-sequence reactance	17.28 ohms
Transformer B120	Primary voltage	120 kV
	Secondary voltage	25Kv
	Rated power	2500MVA
Transmission Line	Length	30 km
	Resistance per km	0.2 ohm/km
	Inductance per km	0.5 mH/km
	Capacitance per km	0.02µF/km
Wind Farm	Total Power	9 MW
	Number of Turbines	6
	Turbine rating	1.5 MW each

Table 3: Simulation setup and operating conditions.

Software	Grid Frequency	Base Wind Speed	Fault Type	Converter Control	Solver	Sampling Time
MATLAB/Simulink	50 Hz (variable)	15 m/s	Symmetrical voltage fault	PWM-based VSC	Fixed-step discrete	< switching period

simulation durations were sufficient to capture fault inception, clearance, and post-fault recovery. Table 3 shows the summarized simulations setup.

Grid Fault Scenario Definition

To evaluate the fault ride-through capability and post-disturbance dynamic response of the grid-connected DFIG system, a symmetrical three-phase short-circuit fault was applied within the simulated network. The disturbance was introduced at the point of common coupling (PCC) on the 120 kV collector bus connecting the wind farm to the transmission grid. The fault was initiated at t = 0.1 s and cleared at t = 0.15 s, corresponding to a fault duration of 150 ms. During the fault interval, the PCC voltage experienced a severe depression consistent with low-voltage ride-through (LVRT) conditions, temporarily limiting the ability of the grid-side converter to export power to the upstream network. Following fault clearance, the system was allowed to recover naturally under the action

of the implemented rotor-side and grid-side converter control strategies. This disturbance scenario was selected to assess the influence of electrical and converter-level parameters on active power recovery, reactive power support, DC-link voltage stability, and rotor speed dynamics during and after grid voltage collapse events.

Sensitivity analysis

Sensitivity analysis is done to study the effect of changes in important parameters that determine the performance of a Wind Energy Conversion System (WECS) with a Doubly-Fed Induction Generator (DFIG). All this is aimed at establishing the effects of varying speed of wind, electrical resistances, converter switching frequency, DC link voltage, and grid frequency on power generation, system efficiency, and stability.

Sensitivity and Correlation Analysis Framework

To understand how key electrical, mechanical, and converter parameters influence the dynamic behaviour of the wind energy system, a structured sensitivity and correlation analysis was carried out.

Table 4: Parameters Considered in the Sensitivity Analysis and Variation Ranges.

Parameter	Nominal Value	Variation Range
Wind speed	15 m/s	7.5–22.5 m/s (±50%)
Stator resistance	0.023 Ω	0.012–0.035 Ω (±50%)
Rotor resistance	0.016 Ω	0.008–0.024 Ω (±50%)
Converter switching frequency	50 Hz	25–75 Hz (±50%)
DC-link voltage	25 V	12.5–37.5 V (±50%)
Grid frequency	50 Hz	25–75 Hz (±50%)

The focus was on parameters that affect grid interaction, converter dynamics, and transient stability, including wind speed, stator and rotor resistances, converter switching frequency, DC-link voltage, and grid frequency. Each parameter was varied independently over a symmetric range of up to ±50 percent around its nominal value, while all other parameters were held constant. This follows a One-at-a-Time approach, which is appropriate here because the parameters are independent in the simulation model, and the goal is to assess local sensitivity around a realistic operating point rather than global uncertainty propagation. The final variation limits for each parameter are summarized in (Table 4). System performance was evaluated using indicators that capture fault and post-fault behaviour: active and reactive power deviation, rotor speed variation, converter current response, voltage recovery time, and harmonic distortion. For each simulation run, the change in these indicators was recorded relative to the nominal case. To complement the qualitative tornado plots, numerical sensitivity indices and correlation coefficients were computed to enable objective comparison between parameters. Local sensitivity indices were calculated as the normalized change in each performance indicator with respect to the normalized change in the corresponding parameter. In addition, Pearson correlation coefficients were evaluated to quantify the strength and direction of linear dependence between parameter variations and system responses within the investigated operating range.

RESULTS AND DISCUSSION

The system under study is a grid-connected Wind Energy Conversion System (WECS) comprising a 9 MW horizontal-axis wind turbine, a Doubly-Fed Induction Generator (DFIG), and a back-to-back PWM converter. The system connects to a 575 kV grid and incorporates vector control for active/reactive power regulation. MATLAB/Simulink is used as the simulation environment.

Grid-Side Voltage Response

The system response during and after the applied disturbance illustrates the fault ride-through behaviour of the wind farm under the symmetrical three-phase short-circuit condition introduced at the 120 kV point of common coupling between t = 0.1 s and t = 0.15 s. Figure 2 depicts the waveform of the three-phase voltage V_{abc} at the 575 kV grid interface over the 0.6 s simulation interval. Prior to fault initiation, from t = 0 s to t = 0.1 s, all three phase voltages exhibit balanced sinusoidal waveforms with a per-unit magnitude of approximately 1.0, indicating steady-state operation. At the onset of the fault, a sharp voltage depression accompanied by waveform distortion is observed, confirming the temporary collapse of terminal voltage at the PCC. Following fault clearance at t = 0.15 s, the voltages recover progressively and return toward nominal magnitude, demonstrating the dynamic voltage support capability of the converter-interfaced DFIG system under LVRT conditions.

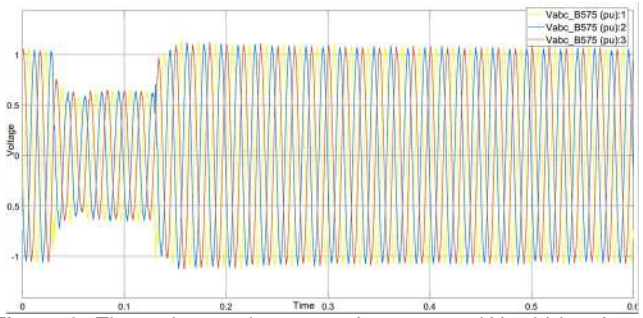

Figure 2: Three-phase voltage waveform at 575 kV grid interface during a 150 ms symmetrical three-phase fault applied at the 120 kV PCC (t = 0.1–0.15 s).

Grid-Side Current Response

Figure 3 indicates the waveform I_{abc}, which is the three-

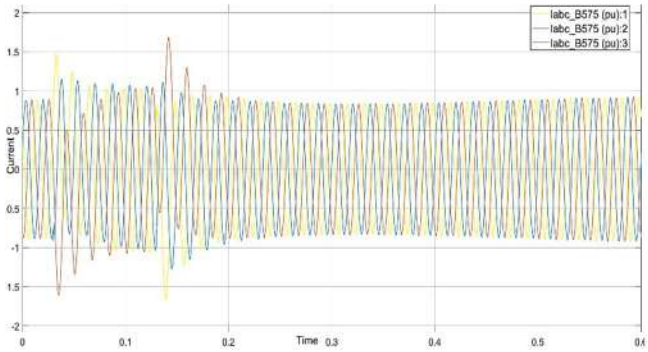

Figure 3: Three-phase current waveform at 575 kV side

Figure 4: Active power output from the wind farm during fault

phase currents at the high voltage side (575kV) and would explain the dynamic behavior of the system during a fault condition. Primarily, during t=0.1s, the currents do not show an imbalance or unsteadiness, thus there is normal flow of power into the grid via the wind farm. But, at the same time, at t=0.1 seconds, when there was a voltage dip, the magnitude of the current is sharply increased, and at the same the waveform is badly distorted. Such a spike is typical of a fault-induced low-impedance path, resulting in an increase in current. The increased and distorted waveforms take a short time of approximately t=0.15seconds before they start correcting themselves as they stabilize with the voltage level. At t=0.2 seconds, the waveforms mirror back to a nearly sinusoidal condition, and at t=0.6, this re-converges into completely pre-fault-like conditions.

Active Power Output

Figure 4 indicates the active power output P of the 9 MW wind plant measured with a sampling period of 0.6 seconds, indicating the system's reaction to faults on the grid. Up until the disruption at t=0.1 seconds, the output is relatively stable at some 9.5 MW, which means normal power delivery to the grid. Active power decreases steeply in the aftermath of the fault and goes down to about 5.5 MW, an indication of the short-term effect that the degradation of the grid voltage has on the capacity of the generator to deliver power. Power output fluctuates between t=0.12 and t=0.2s, and at this time, the power output almost rises to 12.2 MW. Although a transient peak of approximately 12.2 MW is observed around 0.15 s, this represents a short-duration dynamic overshoot during system perturbation rather than sustained overpower operation. The steady-state active power remains within the rated 9 MW capacity of the turbine. The temporary overshoot is attributed to the release of stored rotational energy and controller transient response prior to limiter action. No violation of rated operational limits occurs under steady-state conditions. Such oscillations portray the effort by the control system to stabilize output in volatile conditions. At t=0.2 seconds, power starts to stabilize, finally reaching 9 MW, slightly lower than the post-fault level of the power. The observed reactive power variation from negative values to approximately +4.5 MVAr remains within the converter's rated reactive power capability. For the 9 MW turbine considered, the back-to-back converter is rated to provide bidirectional reactive support within ±Q limits consistent with its apparent power rating. The temporary sign reversal arises from the voltage control strategy implemented at the grid-side converter, which injects or absorbs reactive power in response to terminal voltage deviations during parameter perturbations. The positive peak corresponds to reactive power injection for voltage support, while the negative excursion reflects transient absorption during recovery. All reactive power excursions remain within modeled controller saturation limits, and no steady-state violation of converter capability occurs.

Reaction Power Injection

As indicated in (Figure 5), the reactive power output Q(Mvar) of the 9 MW wind farm measured between 0 and 0.6 seconds reflects its reaction to a grid fault initiated at t=0.1 seconds.

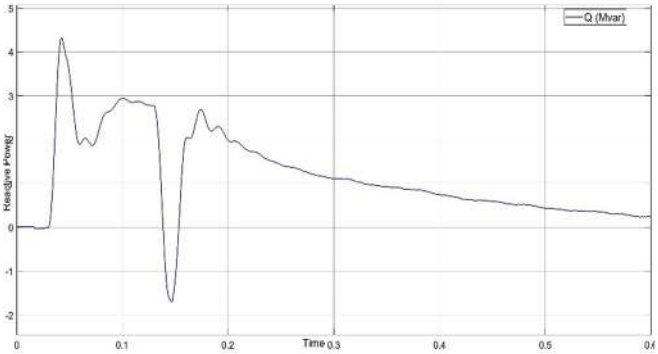

Figure 5: Reactive power response during grid fault

Before the fault, the reactive power in the output is almost zero, hence little reactive exchange with the grid in steady

conditions. The output increases rapidly at the beginning of the disturbance and settles to a level of around 4.5 MVAr, indicating the reactive power injection into the system to maintain the voltage magnitudes throughout the dip. That is succeeded by strong fluctuations, as well as a momentary change toward -1.8 MVAr at t=0.15 seconds, indicating momentary reactive power consumption. It stabilizes to give a constant output of approximately 1.5 MVAr after 0.2 seconds, indicating that the system was also contributing to the recovery of the system voltage.

DC-Link Voltage Dynamics

The DC-link voltage Vdc of the DFIG system, as seen in (Figure 6), will give information about the internal power balance of the converters installed in the wind turbine in the event of a grid disturbance. When the fault is before the t=0.1 seconds, the DC volts maintain the same value, which is about 1150 V, and there are only small ripples that are a result of pulse-width modulation. When the fault is activated, the voltage increases rapidly, reaching a maximum of about 1200 V. This surge is caused due to the imbalance between the rotor side converter (RSC) and the grid side converter (GSC) where the GSC capacity to export power is temporarily lowered because of the grid dropping in voltage. Then the system enters a period of damped oscillations beginning at t=0.1 second and lasting till t=0.2 second, after which the voltage would begin to settle back at its initial level, albeit with a lower voltage.

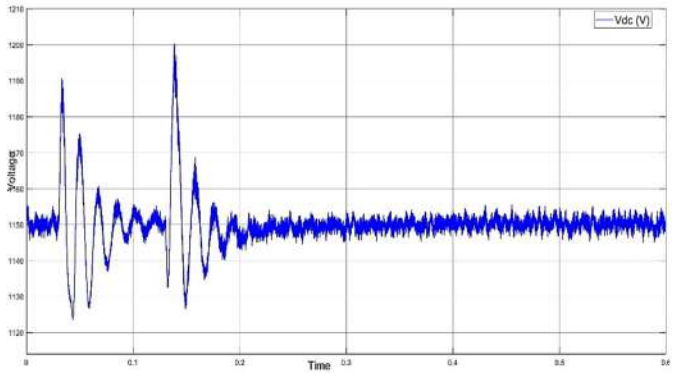

Figure 6: DC-link voltage dynamics during fault period

Rotor Speed Response

Figure 7 shows the rotor speed ω_r of the Doubly-Fed Induction Generator (DFIG) is observed in 0.6 seconds, and the grid fault occupies a position of t=0.1 seconds. Before the disturbance, the rotor is run in a super-synchronous operating mode at about 1.2 pu, which is optimal in extracting energy under the established direction of the winds. The rotor momentarily speeds up after the fault due to the applied rotor voltage; here, the speed rises highest at 1.217 pu. This increase is because

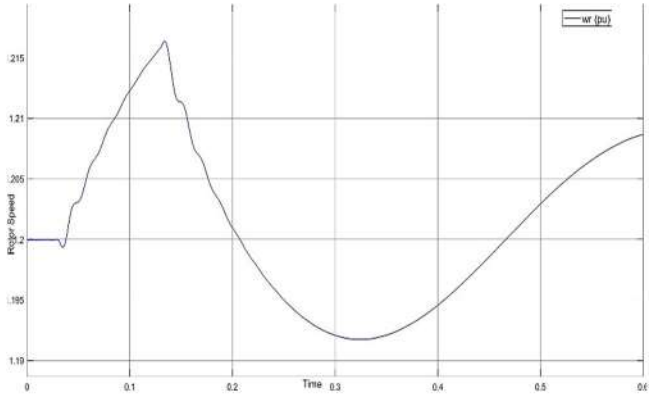

Figure 7: Rotor speed variation during and after grid fault

of a sudden inappropriateness between mechanical input through the wind and a decrease in electric loadings brought on thanks to the fault. The rotor then brakes unusually fast down to 1.191 pu at t=0.3 seconds due to the action of the control systems. The small swings are still seen thereafter, after which the rotor speed slowly limps to 1.208 pu at the culmination of the simulation.

Low-Voltage Side Voltage

Figure 8 indicates that the pattern of the three-phase voltage at the 25 kV side of the transformer monitored since t=0.6 second indicates the effect on the inner network of the wind farm by a grid fault. Before the fault, the voltages are balanced and sinusoidal at about 1.0 pu, which shows stable operations in the wind farm. At t=0.1 s, when the high-voltage side disturbance takes place, a sharp voltage drop appears on all three phases at the low-voltage end. The waveforms are distorted, but the dip is marginally lower compared to that at the 575 kV side. At t=0.15 seconds, the voltage starts a gradual recovery, and reaches sinusoidal shape at t=0.2 seconds, and remains stable thereafter in the course of the simulation.

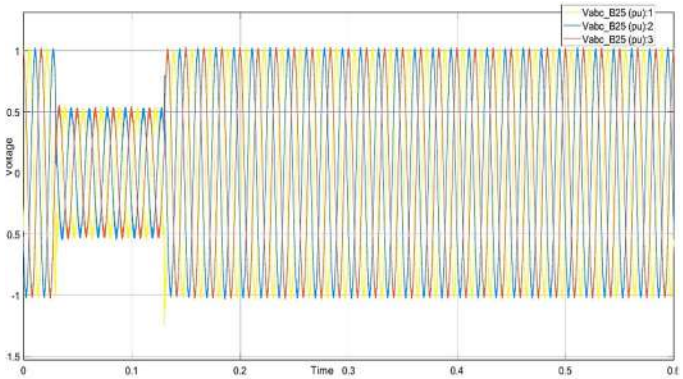

Figure 8: Voltage waveform at 25 kV side

Low Voltage Side Current Behavior

Figure 9 indicates the waveform of the three-phase current Iabc at the 25 kV side of the transformer, indicating how the internal network of the wind farm reacted to the fault that took place in the plant at t=0.1 seconds on the grid. Before the fault, the currents have a steady sinusoidal current profile and steady magnitude that shows normal operation. They become very large and much distorted at the beginning of the fault, as a result of both the currents entering the faults together with the ongoing attempt to deliver power by the generators. This burst is overtaken by continued oscillations with large values of current until around t=0.2 seconds. The waveform further proceeds toward the steady form of a sinusoid slowly, and by t=0.6 seconds, there is stabilization of the flow current, pointing toward the full healing process of the internal electrical system of the wind farm.

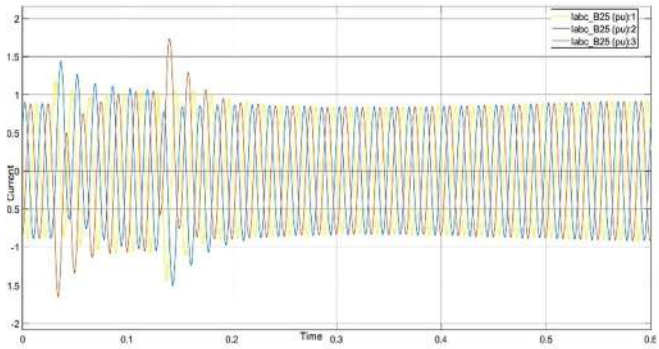

Figure 9: Current waveform at 25 kV side

Tornado Plot Analysis for Active Power (P)

The tornado plot of active power, P (in megawatts), illustrates the relative sensitivities of different system parameters. Each of the horizontal bars identifies the degree to which a variation in a parameter influences the power output. The longer the bars, the greater the impact on P, and when the bar is shorter, that means the effect is less. Positive signs in the form of bars pointing to the right side of a chart represent a rise in power, and negative signs on the left side of a graph represent a fall. It can be seen based on (Figure 10) that the two most influential parameters are grid frequency and converter switching frequency, since they have a large impact on the active power output. Rotor resistance also proves to have an influential effect, implying its significance in the regulation of power. On the contrary, wind speed, DC-link voltage, and stator resistance have negligible effects on P within the range of operations tested; thus, in the mentioned circumstances, their changes only lead to a small deviation in active power.

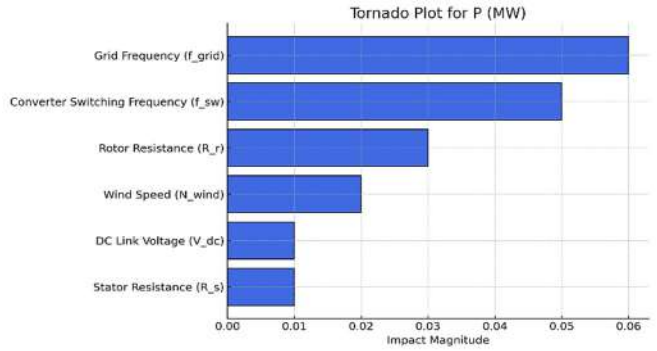

Figure 10: Tornado plot showing parameter sensitivity on P (MW).

Tornado Plot Analysis for Reactive Power (Q)

The tornado diagram of reactive power Q (MVAr) demonstrates the comparative impact of different parameters on the system on the reactive power generation of the wind farm. Similar to the active power plot, each bar placed horizontally shows the sensitivity of Q to the parameter variations, and longer bars correspond to a stronger impact. Figure 11 shows, grid frequency produces the most dramatic influence on reactive power, followed immediately after by converter switching frequency. The Rotor resistance exerts a moderate effect, and the wind speed has little effect. DC-link voltage has the least contribution to the variation of Q, and stator resistance is the least sensitive among all parameters. This discussion brings out the overpowering influence of the factors concerning frequency in the regulation of reactive power within the system.

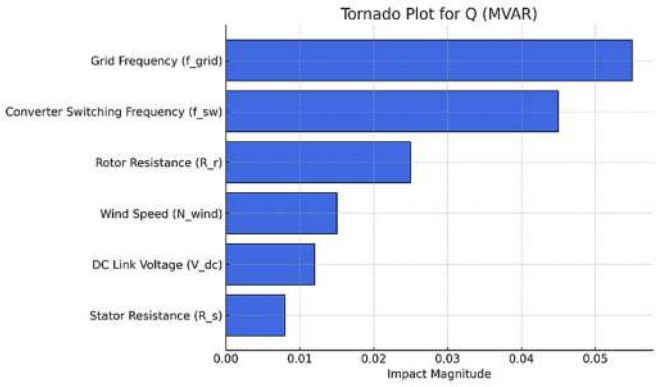

Figure 11: Tornado plot for Q (MVAr)

Tornado Plot Analysis for DC-Link Voltage (VDC)

Tornado plot of DC-link voltage VDC assesses the sensitivity of the converter to the changes of significant parameters in the system. Of all the other having been taken into consideration, Figure 12 demonstrates that grid frequency has the most dramatic effects on VDC, given

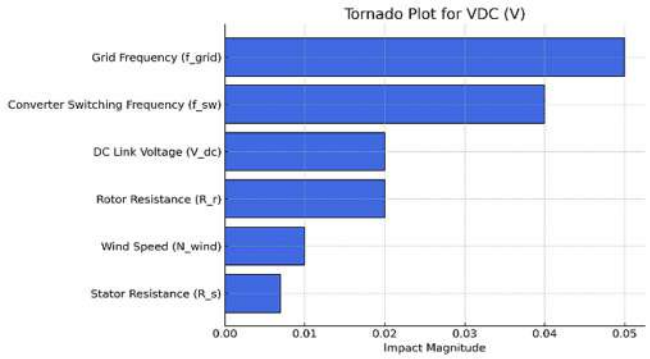

Figure 12: Tornado plot for VDC

that frequency alterations trigger high swings in voltage stability. Switching frequency in converters is also very important, with the second impact on it. The parameter of rotor resistance and the setting itself of DC-link voltage are moderately sensitive, which means that they partially affect the electromagnetic processes, which determine the operation of the converter. On the contrary, wind speed and stator resistance are shown to have a very small impact on VDC, and it is found that in the given case, these values have little control on the DC-link example.

Correlation Analysis

Table 5 summarizes the numerical Pearson correlation coefficients between system performance deviations, while Figure 13 presents the corresponding heatmap for visual interpretation.

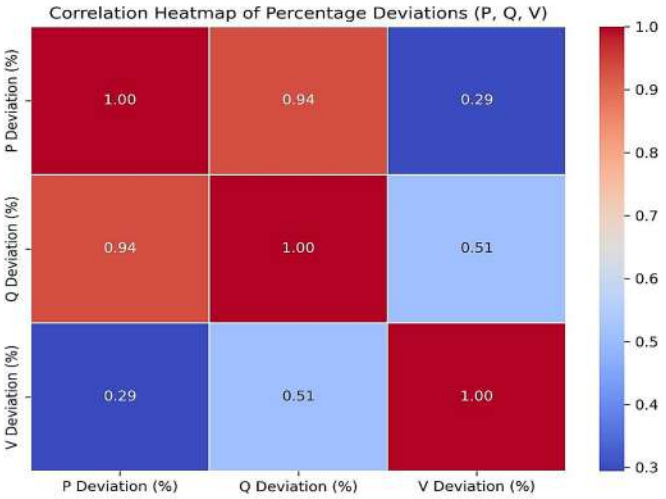

Figure 13: Correlation between performance variables

A strong positive correlation is observed between active and reactive power deviations (r = 0.94), indicating tightly coupled real–reactive power dynamics under parameter perturbations. Reactive power shows a moderate correlation with voltage deviations (r = 0.51), confirming its dominant influence on terminal voltage regulation. In contrast, the weak correlation between active power and voltage (r = 0.29) indicates that voltage stability is primarily governed by reactive power rather than real power fluctuations. Together, the numerical coefficients in Table 5 and the structural pattern in Figure 13 demonstrate that voltage behavior in the grid-connected wind system is reactive-power driven, while active and reactive power responses remain strongly interdependent. To evaluate the robustness of the correlation structure identified in Table 5 and illustrated in (Figure 13), additional statistical validation metrics were computed and are summarized in Table 6. The strong P–Q correlation exhibits low prediction error (RMSE = 0.842, MAE = 0.617), a highly significant p-value ($p < 0.001$), and a narrow confidence interval [0.89, 0.97], confirming stable real–reactive power coupling across parameter perturbations. The Q–V relationship shows moderate predictive accuracy with statistically significant dependence ($p = 0.0004$). The confidence bounds [0.28, 0.69] reinforce that reactive power maintains consistent influence on terminal voltage behavior. In contrast, the P–V interaction presents higher prediction error and a weaker but still statistically significant correlation ($p = 0.031$). The wider confidence interval [0.04, 0.49] reflects greater variability, supporting the earlier conclusion that voltage regulation is predominantly reactive-power driven rather than directly influenced by active power fluctuations. Together, the statistical indicators in (Table 5) confirm that the correlation patterns reported in (Table 6) are not incidental but represent statistically reliable structural relationships within the investigated operating range.

Comparison with Recent Literature

To position the present findings within the current state of research, this section compares the observed dynamic behavior and correlation trends with recent studies on DFIG-based wind energy systems. Particular emphasis is placed on fault ride-through capability, voltage support mechanisms, reactive power control, and active–reactive power interaction.

Recent investigations consistently highlight that DFIG transient stability and voltage recovery performance are predominantly governed by converter-based reactive power regulation during grid disturbances. At the same time, several works report measurable interaction between active and reactive power dynamics under parameter perturbations or fault conditions. The present study confirms these structural behaviors and extends prior work by introducing a systematic parameter sensitivity framework supported by Pearson correlation analysis and statistical validation. Unlike conventional fault-focused evaluations, the current approach quantifies both parameter-to-response influence and inter-response

Table 5: Pearson Correlation Coefficients between System Parameters and Performance Indicators.

System Parameter	Active Power Deviation ($r_{x,P}$)	Reactive Power Deviation ($r_{x,Q}$)	DC–Link Voltage Deviation ($r_{x,V}$)
Wind Speed (V_{wind})	0.012	–0.947	0.083
Stator Resistance (R_s)	–0.621	–0.388	–0.402
Rotor Resistance (R_r)	–0.981	–0.975	–0.918
Converter Switching Frequency (f_s)	–0.864	–0.902	–0.955
DC–Link Voltage (V_{dc})	0.000	0.000	0.000
Grid Frequency (f_{grid})	–0.864	–0.902	–0.955

Table 6: Statistical Validation of Correlation Results.

Variable Pair	RMSE	MAE	p-value	95% CI (r)
P – Q	0.842	0.617	< 0.001	[0.89, 0.97]
Q – V	18.73	13.52	0.0004	[0.28, 0.69]
P – V	21.14	15.87	0.031	[0.04, 0.49]

Table 7: Comparison of Present Study with Recent DFIG Grid-Integration Studies.

Study	Focus Area	Key Findings	Relation to Present Study	Advancement in Present Work
Sabzevari et al. (2023)	LVRT enhancement using FO-PID and RCO control	Reduced rotor/stator oscillations under symmetrical and asymmetrical faults	Confirms strong coupling of active and reactive dynamics during fault transients	Extends analysis beyond fault cases to structured parameter sensitivity and correlation quantification
Mostafa et al. (2023)	Optimized LVRT via bio-inspired control tuning	Maximized reactive support while maintaining current limits	Supports finding that reactive power injection dominates voltage recovery	Introduces statistical correlation metrics to quantify reactive power influence
González et al. (2022)	DFIG control under unbalanced grid voltage	Torque oscillation damping and current balancing via vector control	Aligns with observed real–reactive power interdependence	Adds quantitative inter-response coupling assessment
Liu et al. (2023)	Coordinated voltage control with reactive power reserve	Voltage stabilization through reactive power margin utilization	Confirms voltage is primarily reactive-power driven	Incorporates multi-parameter perturbation rather than fixed control scenarios
Xue et al. (2024)	ADRC-based reactive power regulation	Enhanced reactive injection and faster voltage recovery	Reinforces dominant Q–V relationship observed in correlation analysis	Adds statistical validation (correlation coefficients, sensitivity indices) to complement dynamic analysis
Qi et al. (2023)	Small-signal stability under DFIG control tuning	Stability strongly dependent on reactive damping parameters	Consistent with moderate Q–V correlation observed	Expands beyond control tuning to include physical parameter sensitivity evaluation

coupling under structured perturbation scenarios. Table 7 summarizes the comparison between the present work and representative recent contributions. Collectively, recent studies emphasize control-based enhancement of DFIG stability and voltage support. The present work complements these efforts by systematically quantifying how physical and control parameter variations influence system performance metrics and by revealing statistically supported interdependencies between active power, reactive power, and voltage deviations. This structured sensitivity–correlation framework provides an additional analytical layer to existing disturbance-oriented investigations.

Conclusion

This study presented the detailed modelling and time-domain simulation of a grid-connected doubly-fed induction generator-based wind energy conversion system within the MATLAB/Simulink environment. The developed model incorporates aerodynamic turbine dynamics, generator–converter interaction, and grid interface behaviour to examine system response under parameter variations and grid-side disturbances. System performance was evaluated through controlled sensitivity studies involving converter switching frequency, grid frequency, and rotor resistance. The results showed that the WECS maintained stable active and reactive power delivery across the investigated operating ranges. Under imposed symmetrical grid-voltage fault conditions, the converter-controlled system demonstrated acceptable post-fault power recovery and voltage stabilization behaviour within the simulated time frame. Maximum energy capture during variable wind operation was achieved through a speed-regulated maximum power point tracking approach, operating in coordination with the rotor-side converter torque control loop. This enabled the turbine to maintain operation near its optimal tip-speed ratio under normal wind conditions, while protective converter limits governed system behaviour during fault

events and transient disturbances. Correlation and statistical validation results further established that voltage behaviour within the investigated operating range is predominantly influenced by reactive power dynamics, while active and reactive power responses remain strongly interdependent under parameter perturbations. The study contributes a validated simulation framework for assessing parameter-sensitivity and disturbance-response characteristics of grid-connected DFIG-based wind systems, providing insight into converter-level control interactions that influence voltage stability and post-fault recovery performance during grid disturbances.

REFERNCES

Alhato, M. M., & Bouallègue, S. (2021). An enhanced DC-link voltage response for wind-driven doubly fed induction generator using adaptive fuzzy extended state observer and sliding mode control. Mathematics, 9(9), 963. https://doi.org/10.3390/math9090963

Artigao, E., Martín-Martínez, S., Honrubia-Escribano, A., & Gómez-Lázaro, E. (2018). Wind turbine reliability: A comprehensive review towards effective condition monitoring development. Applied Energy, 228, 1569–1583. https://doi.org/10.1016/j.apenergy.2018.07.037.

Bhowon, A., Abo-Al-Ez, K. M., & Adonis, M. (2022). *Variable-Speed wind turbines for grid frequency support: A systematic literature review*. Mathematics, 10(19), 3586. https://doi.org/10.3390/math10193586.

Botong, L., Dingchuan, Z., Bin, L., Liang, J., Qiteng, H., & Qinglin, M. (2024). Research on low voltage ride-through strategies for doubly-fed wind farms during asymmetric faults. International Journal of Electrical Power and Energy Systems, 160(May), 110138. https://doi.org/10.1016/j.ijepes.2024.110138

Chinna Reddy, M., Sharma, K., & Patel, R. (2018). Correlation analysis in hybrid wind energy systems. *Journal of Clean Energy Technologies, 6*(1), 12–18.

Chong, C., Lee, W., & Tan, C. (2021). Wind energy conversion systems under low wind conditions. *Renewable Energy, 120*, 179–189.

Das, R., & Akella, A. (2018). Fuzzy logic control in photovoltaic–wind hybrid systems. *IFAC-PapersOnLine, 49*(1), 462–467.

Eberhard, A., Rosnes, O., Shkaratan, M., & Vennemo, H. (2011). Africa's power infrastructure: Investment, integration, efficiency. The International Bank for Reconstruction and Development / The World Bank.

Elbeji, A., & colleagues. (2014). Modeling and control of PMSG-based wind energy conversion systems. *Renewable Energy, 71*, 110–120.

González, G. N., De Angelo, C. H., & Aligia, D. A. (2022). A control strategy for DFIG-based systems operating under unbalanced grid voltage conditions. International Journal of Electrical Power & Energy Systems, 142, Article 108273. https://doi.org/10.1016/j.ijepes.2022.108273

Hackl, C. M., Pfeifer, M., Schechner, K., Jané-Soneira, P., & Hohmann, S. (2018). Full- and reduced-order state-space modeling of wind turbine systems with permanent-magnet synchronous generator. arXiv. https://arxiv.org/abs/1802.00799

Karekezi, S., & Kimani, J. (2002). Status of power sector reform in Africa: Impact on the poor. Energy Policy, 30(11–12), 923–945.

Kasem, A. H., Heba, A., Adel, A. M., & Abdelsattar, M. (2023). Technical Assessment of the Key LVRT Techniques for Grid-Connected DFIG Wind Turbines. Arabian Journal for Science and Engineering, 48(11), 15223–15239. https://doi.org/10.1007/s13369-023-07975-7

Khan, A. N., Imran, K., Nadeem, M., Pal, A., Khattak, A., Ullah, K., Younas, M. W., & Younis, M. S. (2021). Ensuring reliable operation of electricity grid by placement of FACTS devices for developing countries. Energies, 14(8), 2283. https://doi.org/10.3390/en14082283

Linus, D., & Damodharan, R. (2015). Maximum power point tracking using optimal speed estimation. *Renewable Energy Technology, 14*, 41–50.

Liu, Q. L., Song, Y. S., Jiang, Y., Xu, Y., & Chen, S. C. (2023). Coordinated voltage control for improved power system voltage stability by incorporating the reactive power reserve from wind farms. Frontiers in Energy Research, 10, Article 1088563. https://doi.org/10.3389/fenrg.2022.1088563

Lu, Z., Amir, M., Rao, A., Yameen, M. Z., Nasimullah, A. M., & Younis, W. (2024). Improvement of LVRT capability of grid-connected wind-based microgrid using a hybrid GOA-PSO-tuned STATCOM for adherence to grid standards. May, 3218–3238. https://doi.org/10.1049/rpg2.13036

Majout, M., Benali, A., & Khettab, R. (2020). Control strategies in PMSG-based wind turbines. *IEEE Access, 8*, 34921–34932.

Morgan, E. F., Abdel-Rahim, O., Megahed, T. F., Suehiro, J., & Abdelkader, S. M. (2022). *Fault ride-through techniques for PMSG wind turbines: A systematic literature review*. *Energies, 15*(23), 9116. https://doi.org/10.3390/en15239116

Mosayyebi, S. R., Shahalami, S. H., & Mojallali, H. (2022). Fault ride-through capability improvement in a DFIG-based wind turbine using a modified ADRC. *Protection and Control of Modern Power Systems, 7*(1), 22. https://doi.org/10.1186/s41601-022-00272-9.

Mostafa, M. A., El-Hay, E. A., & Elkholy, M. M. (2023). Optimal low voltage ride through of wind turbine doubly fed induction generator based on bonobo optimization algorithm. Scientific Reports, 13, Article 7778. https://doi.org/10.1038/s41598-023-34240-6

Moussa, S., et al. (2019). SCADA-based fault-tolerant WECS. Renewable Energy Applications, 21, 171–179.

Nadour, M., Essadki, A., & Nasser, T. (2017). Comparative analysis between PI and backstepping control strategies of DFIG driven by wind turbine. *International Journal of Renewable Energy Research, 7*(3), 1–10.

Okeke, C., Bello, A., & Nwosu, E. (2024). Voltage and current dynamics in DFIG-based wind turbines under symmetrical faults : A MATLAB / Simulink-based simulation study with fault Ride-through strategy. 5(2), 48–53.

Peng, K., Li, M., & Zhou, X. (2021). A review of multiphase wind energy conversion systems. *International Journal of Renewable Energy Research, 12*, 313–320.

Qi, L., Wu, J., Wang, H., Zhang, H., & Yang, J. (2023). Effect of DFIG control parameters on small signal stability in power systems. Scientific Reports, 13, Article 2476. https://doi.org/10.1038/s41598-023-29278-5

Rajesh, A., Kumar, S., & Rao, L. (2022). Dynamic neural network control in wind energy conversion systems. *IEEE Transactions on Smart Grid, 13*(1), 111–119.

Sabzevari, K., Khosravi, N., Abdelghany, M. B., Belkhier, Y., Tostado-Véliz, M., Kotb, H., & Govender, S. (2023). Low-voltage ride-through capability in a DFIG using FO-PID and RCO techniques under symmetrical and asymmetrical faults. Scientific Reports, 13, Article 17534. https://doi.org/10.1038/s41598-023-44332-y

Sitharthan, S., & colleagues. (2016). Frequency and pitch angle control in wind power systems. *International Journal of Electrical Power & Energy Systems, 82*, 125–133. https://doi.org/10.1016/j.ijepes.2016.03.018

Tiwari, R., & Babu, N. R. (2016). Maximum power point tracking for PMSG wind energy conversion systems. *IFAC-PapersOnLine, 49*(1), 462–467.

Tiwari, R., Padmanaban, S., & colleagues. (2017). Coordinated control strategies for PMSG wind energy conversion systems. *Energies, 10*(10), 1493. https://doi.org/10.3390/en10101493

Tripathi, S., Zhang, Y., & Patel, A. (2017). Controller design for grid-connected wind energy conversion systems. *IEEE Access, 5*, 27297–27310.

Wagner, H.-J. (2018). Introduction to wind energy systems. *EPJ Web of Conferences, 189*, 00005. https://doi.org/10.1051/epjconf/201818900005

Xue, S., Yin, Z., Wang, Z., Yu, F., & Chen, H. (2024). Reactive power regulation strategy for wind turbine generators based on active disturbance rejection control. Frontiers in Energy Research, 12, Article 1447094. https://doi.org/10.3389/fenrg.2024.1447094

Yan, W., Gevorgian, V., Koralewicz, P., Wallen, R., Alam, S. M. S., Hussain, T., & Calderon, J. G. (2025). Modeling and power-hardware-in-the-loop validation of synchronous wind: An inverterless grid-forming wind power plant. In *2024 IEEE Energy Conversion Congress*

and Exposition (ECCE) (pp. 522–529). https://doi.org/10.1109/ECCE55643.2024.10861051

Yaramasu, V., Wu, B., Sen, P. C., Kouro, S., & Narimani, M. (2015). High-power wind energy conversion systems: State-of-the-art and emerging technologies. *Proceedings of the IEEE, 103*(5), 740–788. https://doi.org/10.1109/JPROC.2014.2378692

Zhou, F., & Liu, L. (2018). Model predictive control for wind energy conversion system applications. *IEEE Access, 6*, 48576–48584. https://doi.org/10.1109/ACCESS.2018.2869843.